ADITYA SAMBAMURTI MEMORIAL LECTURE

Creating High Density Matters at AGS Energies

Ziping Chen

Department of Physics

Brookhaven National Laboratory

Upton, NY 11973

July 29, 1996

1. Introduction

In this lecture, I discuss high baryon density nuclear matter created in head-on collisions of Au+Au at AGS energies. The questions I will try to answer are: why is high density matter interesting? how do we convince ourselves that high density matter has been formed in our laboratory studies? and finally what is the impact on our future research?

2. Nuclear Matter At High Baryon Density

In the physical world, nuclear matter exists at different scales in dimension, from the microscopic to the macroscopic. At the microscopic level are the various nuclei, for example the Helium nucleus and the Lead nucleus as indicated in Fig. 1. Their typical sizes are of the order of a few Fermi (1 Fermi = 10^{-15} Meter). On the other end of this spectrum are the macroscopic objects called neutron stars, whose typical sizes are about 10 km. In between no object has been discovered, and for this reason the term “nuclear desert” has been coined [1]. As in condensed matter physics, an equation of state can be invoked to describe the properties of nuclear matter in different phases. The details of such an equation of state are still poorly known but there are strong theoretical reasons to believe that several distinct phases exist for nuclear matter [2]. In Fig. 2, nuclear matter has been categorized in three regions on the phase diagram: the hadronic phase, the mixed phase, and the quark gluon plasma phase. The nuclei exist at the point in the phase diagram called normal nuclear matter, and they are like droplets of liquid of different size

with more or less the same density . The neutron stars have very low temperature, and their density could reach as high as about 5 times normal nuclear matter density in their cores.

There has been tremendous interest in reaching the phase of the quark gluon plasma through the collision of heavy ions in the laboratory. The main difference between hadronic matter and the quark gluon plasma is how the quarks are confined. We know hadrons contain valence quarks—mesons (π^- , π^+ ...) have two and baryons (protons, neutrons, ...) have three. Each hadron is like a "bag" in which quarks move almost freely but never get out. In other words quarks are confined inside the bags. Hadronic matter is made of these hadrons which confine their constituent quarks inside, as depicted on the left hand side of Fig. 3. On the other hand, in the quark gluon plasma, quarks are free inside the whole plasma and there are no "bags" to confine them. The existence and the properties of the quark gluon plasma are fundamental to the current understanding of the strong interaction, primarily formulated in the theory of QCD (Quantum Chromo Dynamics), and the experimental search for the quark gluon plasma is well under way both at the AGS of Brookhaven and at the SPS of CERN, and will go into full swing with the operation of RHIC (Relativistic Heavy Ion Collider) at BNL. In a very simple picture one can conceive two ways to create such a form of matter in the laboratory, one by high baryon density along the x-axis of the phase diagram and another by high temperature along the y-axis. Of course any combination of the two will work too. One applies pressure to create the high density matter as depicted in Fig. 4. When the pressure is sufficiently high, the space between the hadrons is filled up and eventually all hadrons overlap in space. The individual bags break up and quarks become free of their confinement. This is the place where the high baryon density matter believed to be created at AGS energies provides opportunities for reaching into the quark gluon plasma phase. The alternative route into the quark gluon plasma is through heating the matter to high temperature as symbolized in Fig. 4, so high that the confining bags of hadrons eventually melt down, liberating quarks from confinement. Hopefully RHIC currently under construction at BNL will realize this condition.

As modeled by ARC (A Relativistic Cascade), the head-on collision of two gold ions at AGS energies goes through a stage of high baryon density, followed by a gradual disintegration and

finally a freeze-out when all the particles involved in the reaction stop interacting with each other. Experimentally we observe only the condition of the reaction after freezing out, and try to learn the whole process of the reaction partly by comparing models such as ARC with experimental observation. As an example of such calculation, Fig. 5 shows the process of reaction by two gold ions. The time when each picture is made is indicated on the top. Before the collision at t=-5fm/c, the two gold ions are contracted in the Z-direction because of their high speed approaching each other. At t=0fm/c when the two nuclei completely overlap, the highest density of the collision process is reached. As time goes further the high density region starts to disintegrate (t=5 fm/c) and eventually freezes out (t=20 fm/c).

3. Experiment E866

Experiment E866 is the one on which I have been working at AGS energies to study the Au+Au reactions. The schematic setup of this experiment is shown in Fig. 6. Basically it can be divided into two parts: global detectors for event characterization and spectrometers for particle detection. There are two global detectors implemented, ZCAL (zero-degree calorimeter) and NMA (new multiplicity array), for centrality definition. The ZCAL measures the remnant energy of the projectile after it goes through a collision, and the NMA counts the number of produced particles in the reaction. Two spectrometers are installed in the experiment with different apertures, and they cover different angular ranges with a total coverage from 6 to 54 degrees in the laboratory.

Figure 7 is an illustration of event characterization by the correlation between the two global detectors. At the lower end of the correlation curve is the peripheral reactions when the two gold nuclei impact at large distance. A significant part of the projectile does not participate in the reaction and dumps its energy in the ZCAL producing a large signal there, and because a small fraction of the incident nuclei are involved in the reaction only a small number of particles are produced, giving rise to a tiny signal in NMA. On the other hand when two gold nuclei collide head on, no projectile remnant is left and a small signal appears in the ZCAL, and a large number of produced particles is detected by the NMA generating a big signal in it. This situation

corresponds to the upper end on the correlation curve. Taking advantage of this correlation, the experimenters can select events of different impact parameters ranging from peripheral to central collisions.

For each selected range of impact parameters, the experimenters can study particle production with the spectrometers. The basic principle of a magnetic spectrometer is illustrated in Fig. 8. A charged particle ionizes gases in the tracking detectors (drift chambers), and its direction is bent by the magnet with the positively charged bent one way and the negatively charged bent oppositely. Its flight time is measured by a wall of scintillators denoted as TOFW. Experimenters can use this information to reconstruct the trajectory of the charged particles, to calculate their momentum based on the degree of their bending, and characterize their identity by calculating their mass.

It is a useful exercise to go through the kinematic variables used to present the experimental results. Since high energy is involved in the experiment and particles travel at relativistic speed close to that of the light, laws of relativity have to be considered in presenting the experimental results so that they will be meaningful in different frames of observation, including the laboratory frame. As indicated in Fig. 9, the experiment measures the momentum, the mass, and the emission angle of each detected particle in the laboratory frame, and transforms these variables into relativistically convenient variables such as transverse mass and rapidity. The same particle will be observed in two different frames of observation along the beam direction with the same transverse mass, m_t, and two different rapidities y and y', where y and y' are related additively $y=y_0+y'$ with y_0 being the relative rapidity of the two observing frames. In the figure, the two frames are specifically chosen as the laboratory frame and the center of mass frame with the relative rapidity of the two frames as $y_0=y_{nn}$. The yield of particle production will be presented as invariant cross section, which is, as its name suggests, invariant under different frames of observation.

With the introduction of the proper kinematic variables, we can start to present our experimental results for the central Au+Au reaction at 11.6 A·GeV/c. At this incident energy, the beam and

target rapidity are 3.2 and 0 respectively, and the rapidity for the center of mass frame is 1.6. In Fig. 10, the invariant yields of protons are presented at several rapidities as a function of transverse mass minus the rest mass of protons, m_t-m_0. The invariant yields are scaled down by a factor of ten successively for increasing δy, where δy is the distance in rapidity from the central rapidity, $\delta y = |y-y_{nn}|$. The solid points are the measurement from the small aperture spectrometer, FS, and the open points are from the large aperture spectrometer, HH. The agreement between the two spectrometers is remarkable. The curves in the figure are fits to the spectra based on a two-exponential function, and the particle yield at each rapidity will be obtained by integrating the curve from its origin to infinity.

In Fig. 11 we concentrate on the spectra at central rapidity y_{nn}=1.6 for central Au+Au reactions. The solid round points are for protons scaled down by a factor of 2, open round points for π^-, and solid squares for π^+. Contrary to previous measured spectra in reactions induced by light ion beams (p, O, Si), none of the spectra is exponential in shape. For protons, the spectrum bends down at low m_t-m_0, and for pions the spectra rise up at low m_t-m_0. π^- rises faster than π^+ does, and the ratio of π^-/π^+ is not flat but rises at low m_t-m_0, as depicted in the insert.

After integrating the spectra over m_t-m_0, one obtains the rapidity distribution of particle yields. The rapidity distribution for baryons contains essential information on the dynamics of the reaction, since at AGS energies baryons produced by pair-production together with an antibaryon are extremely rare and almost all the baryons are redistributed by the reaction process from the original projectile and the target. Fig.12 shows the rapidity distribution of protons and pions from the very simple reaction of p+p to the most complex reaction of central Au+Au reactions. The horizontal axis is the rapidity normalized to the beam rapidity, and the vertical axis is the yield, dn/dy. For protons, the rapidity distribution for p+p has two peaks around projectile and target rapidities respectively, indicating that most of the protons keep traveling at almost the same rapidities before and after the collision, little stopped by the reaction. The situation does not change significantly for peripheral collisions of Al+Si, and in central Al+Si there is significant shifting in rapidity away from the projectile and the target, but a hole in the central rapidity still exists. Only in the central Au+Au reactions, due to the large size of the gold

ions, are protons almost completely stopped around central rapidity, filling up the hole in the middle. The same distributions for pions, however, stays more or less the same shape regardless of the size of the incoming projectile and target.

When the protons are substantially stopped, it sets the scene for creating high baryon density matter in the course of the reaction. The data indicate that in central Au+Au reactions the highest density has been reached, but unfortunately no direct measurement is possible as to the exact value of the density. Model comparison has to be utilized in order to extract this number from the experiment. As a prediction, the ARC model produced the correct rapidity distribution for protons in the central Au+Au reactions as indicated in Fig. 13. In order to produce such a rapidity distribution, the reaction has to go through a stage of high baryon density when the two nuclei completely overlap, and this density is as high as 5 or 6 times the normal nuclear matter density. This is the highest density reached in the laboratory by the collision of two atomic nuclei, and many interesting phenomena are expected to occur in such a high baryon density environment, including a phase transition to the quark gluon plasma. While the experimental search for the signal of such a transition is still under way, so far there is no direct observation for the transition yet. Besides the phase transition, other interesting topics are also under study, including the production and annihilation of anti-protons in the high density medium, the possible production of stranglets, mass shifts of particles in the high density medium, and flow properties and information on the nuclear equation of state.

4. Baryon Distribution at RHIC Energies

It is still a open question to what degree the stopping will occur at RHIC energies. Transparency of the two nuclei was expected earlier, but recent model calculations extrapolated to RHIC energies indicate otherwise. The net baryon distribution at central rapidity varies from model to model as illustrated in Fig.14, indicating an uncertainty in the current understanding of the collision dynamics. Ultimately the question needs to be settled experimentally, for which a small RHIC experiment called Brahms (Broad RAnge Hadron Magnetic Spectrometers) is proposed. Unlike other experiments at RHIC, the Brahms experiment features a large coverage in phase

space with exceptional particle identification as indicated in Fig.15. This is realized by two spectrometers, a small aperture forward arm and a large aperture mid-rapidity arm, in addition to event characterization detectors. The schematic layout of the experiment is shown in Fig. 16. To learn more about Brahms one can surf its home page: http://www.rhic.bnl.gov/export1/brahms/WWW/brahms.html

5. Summary

In summary we have evidence of reaching high baryon density in the course of head-on collisions of two gold ions. This is obtained by comparing the rapidity distribution of protons from very simple collisions of p+p, where little stopping is observed, to the central Au+Au reactions, where most of the participating protons pile up around the central rapidities. The conclusion is reinforced by model calculations such as ARC in which the collision goes through a high density stage, of the order of 5 or 6 times normal nuclear matter density, when the two nuclei complete overlap. At RHIC energies the question of stopping has to be resolved experimentally, and Brahms experiment is poised to play its role there.

References:

[1] H. Crawford and C. H. Greiner, Scientific American, 72 Jan. 1994

[2] The Nuclear Equation Of State, Part B: QCD and the formation of the quark gluon plasma. Edited by Walter Greiner and Horst Stocker. Plenum Press, 1989.

Figure Captions:

Figure 1. An illustration of the landscape of nuclear matter.

Figure 2. A schematic phase diagram of nuclear matter. There are three phases indicated in the diagram: hadronic matter, the mixed phase, and the quark gluon plasma. The arrows are expected

routes which reactions at the corresponding energies might take to reach the quark gluon plasma phase.

Figure 3. An illustration of the difference between hadronic nuclear matter and the quark gluon plasma.

Figure 4. Two simple minded ways to reach the quark gluon plasma in the laboratories, one by high pressure and another by high temperature.

Figure 5. A model simulation of central Au+Au reactions at AGS energies by ARC (A Relativistic Cascade). The time when the snap shots are taken is indicated on top of each picture. The solid points represent particles in their excited state.

Figure 6. Schematic setup of experiment E-866**.**

Figure 7. Correlation between ZCAL (zero degree calorimeter) and NMA (new multiplicity array) in E866 for Au+Au reactions at 11.6 A·GeV/c. As explained in the text, the regions corresponding to central and peripheral reactions are indicated**.**

Figure 8. The basic principle of the E866 magnetic spectrometers.

Figure 9. Kinematic variables in the measurement and for data presentation.

Figure 10. Invariant yields for produced protons in central Au+Au reactions at 11.6 A·GeV/c. The spectra are scaled down successively by a factor of 10 for presentation.

Figure 11. The invariant yields for protons, π^- , and π^+ at central rapidity y_{nn} in central Au+Au reactions at 11.6 A·GeV/c.

Figure 12. Proton and pion rapidity distributions from p+p reactions to central Au+Au reactions at AGS energies. The rapidity on the x-axis is normalized to the beam rapidity.

Figure 13. Comparison of proton rapidity distribution between a model calculation by ARC and the data from E866. The agreement is remarkable.

Figure 14. Various predications for baryon and meson rapidity distributions at RHIC energies. The discrepancy among the models is large, and needs to be settled experimentally.

Figure 15. The proposed coverage by Experiment Brahms. Unlike any other RHIC experiments, Brahms features a large coverage for hadronic particles.

Figure 16. The experimental layout of the Brahms experiment.

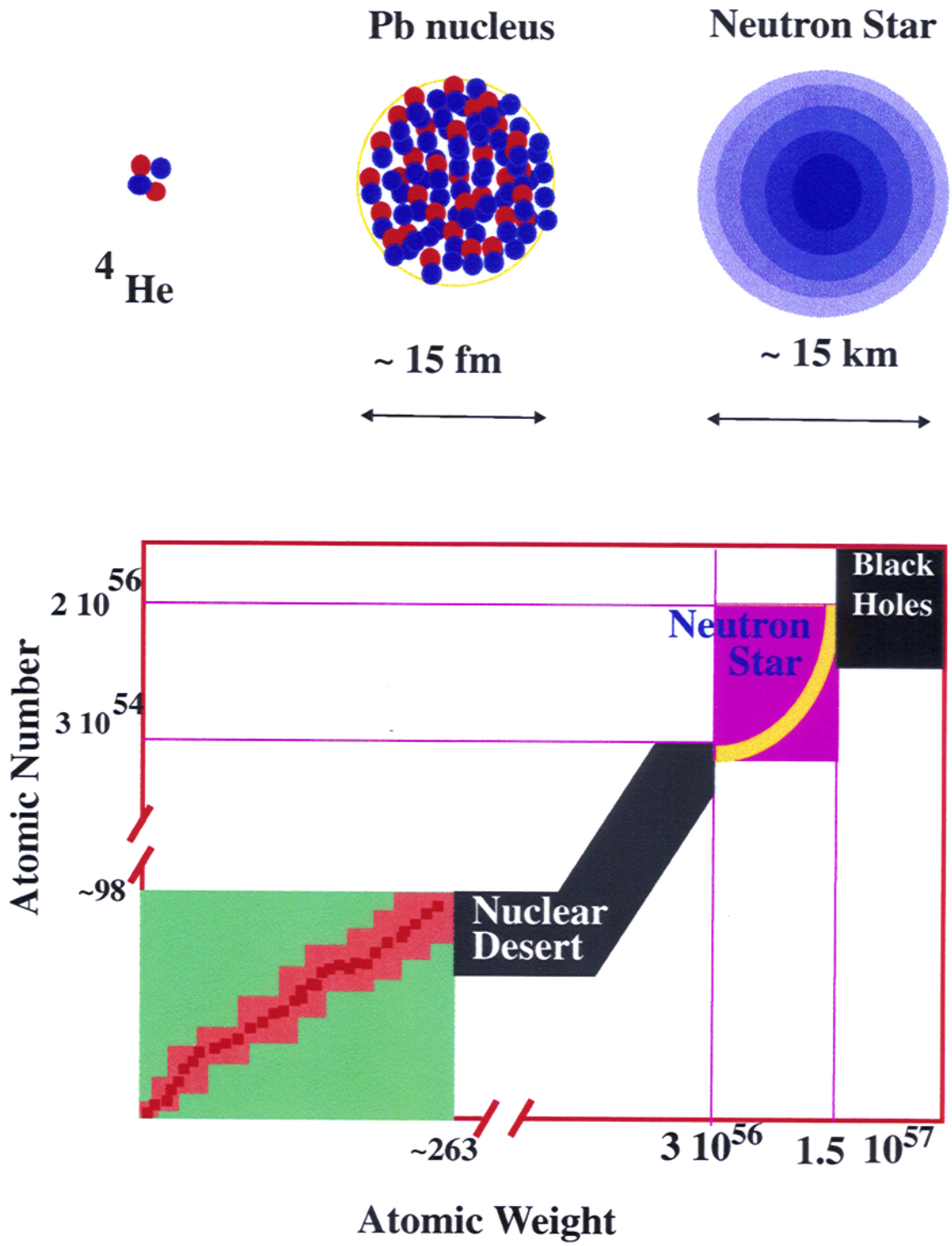
Pb nucleus
Neutron Star
4 He
~ 15 fm
~ 15 km
Black Holes
Neutron Star
Nuclear Desert
Atomic Number
2 10^56
3 10^54
~98
~263
3 10^56
1.5 10^57
Atomic Weight

Figure 1

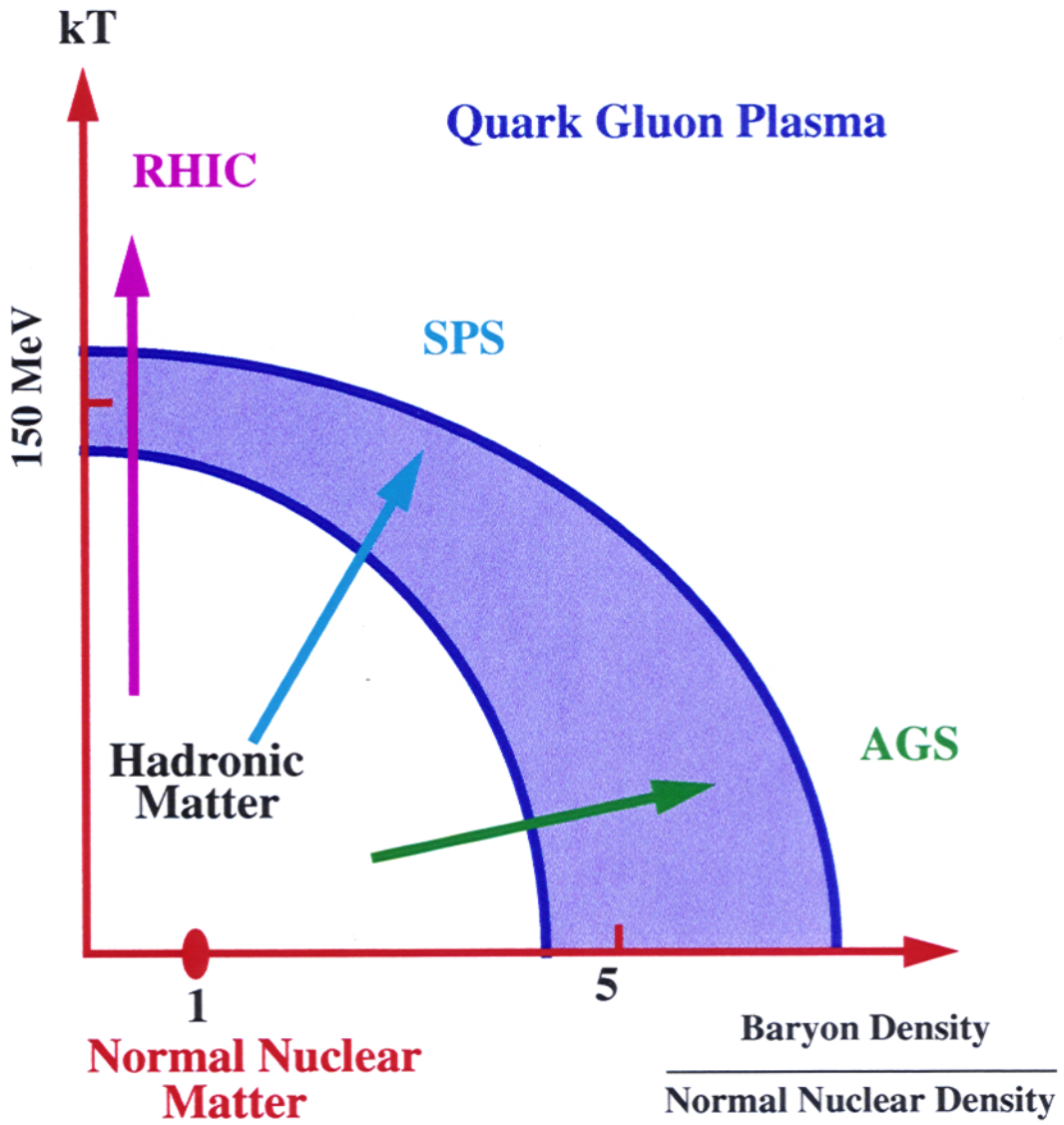
kT
Quark Gluon Plasma
RHIC
150 MeV
SPS
Hadronic
Matter
AGS
1
5
Normal Nuclear
Matter
Baryon Density
Normal Nuclear Density

Figure 2

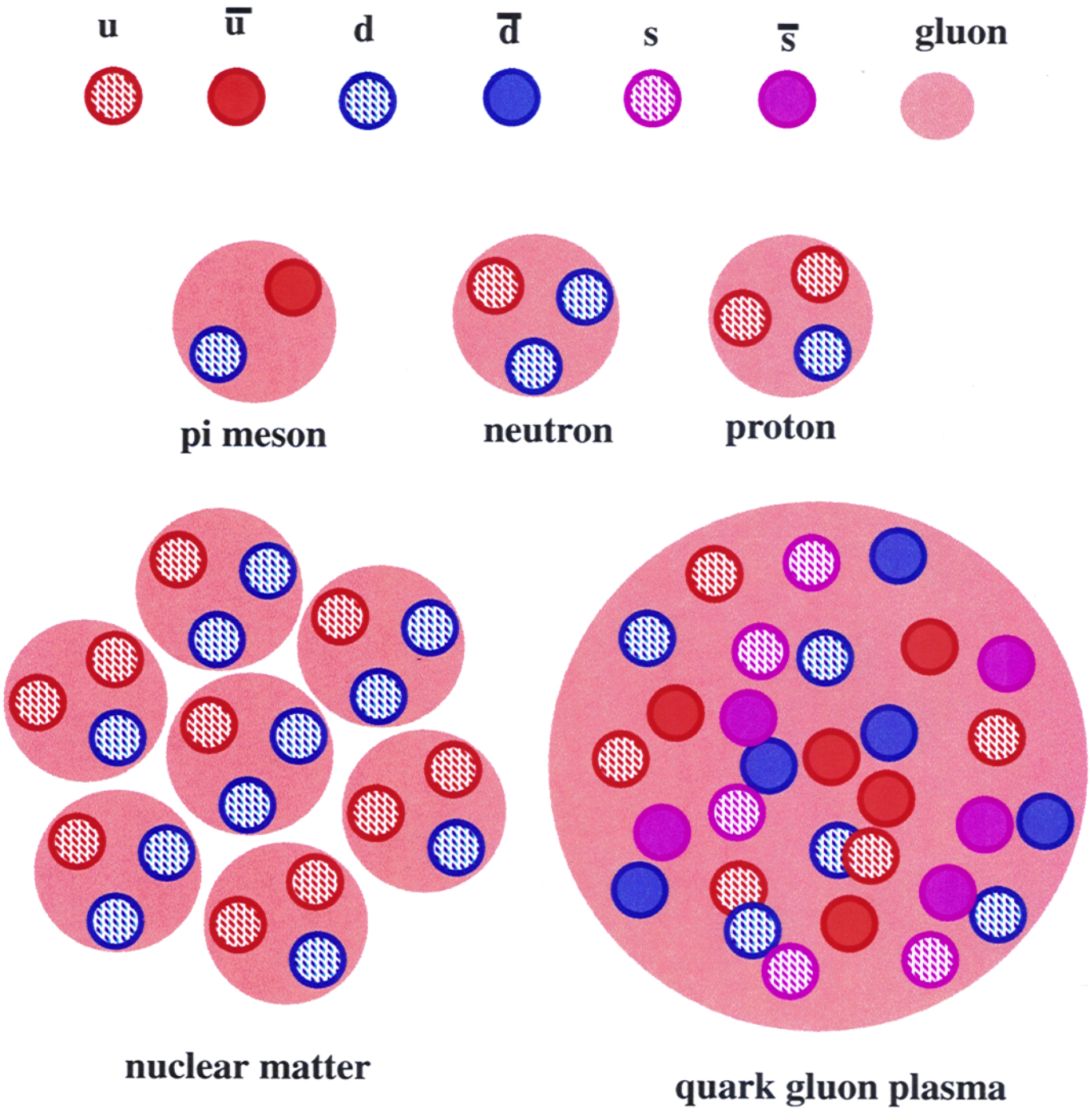
u
ū
d
d̄
s
s̄
gluon
pi meson
neutron
proton
nuclear matter
quark gluon plasma

Figure 3

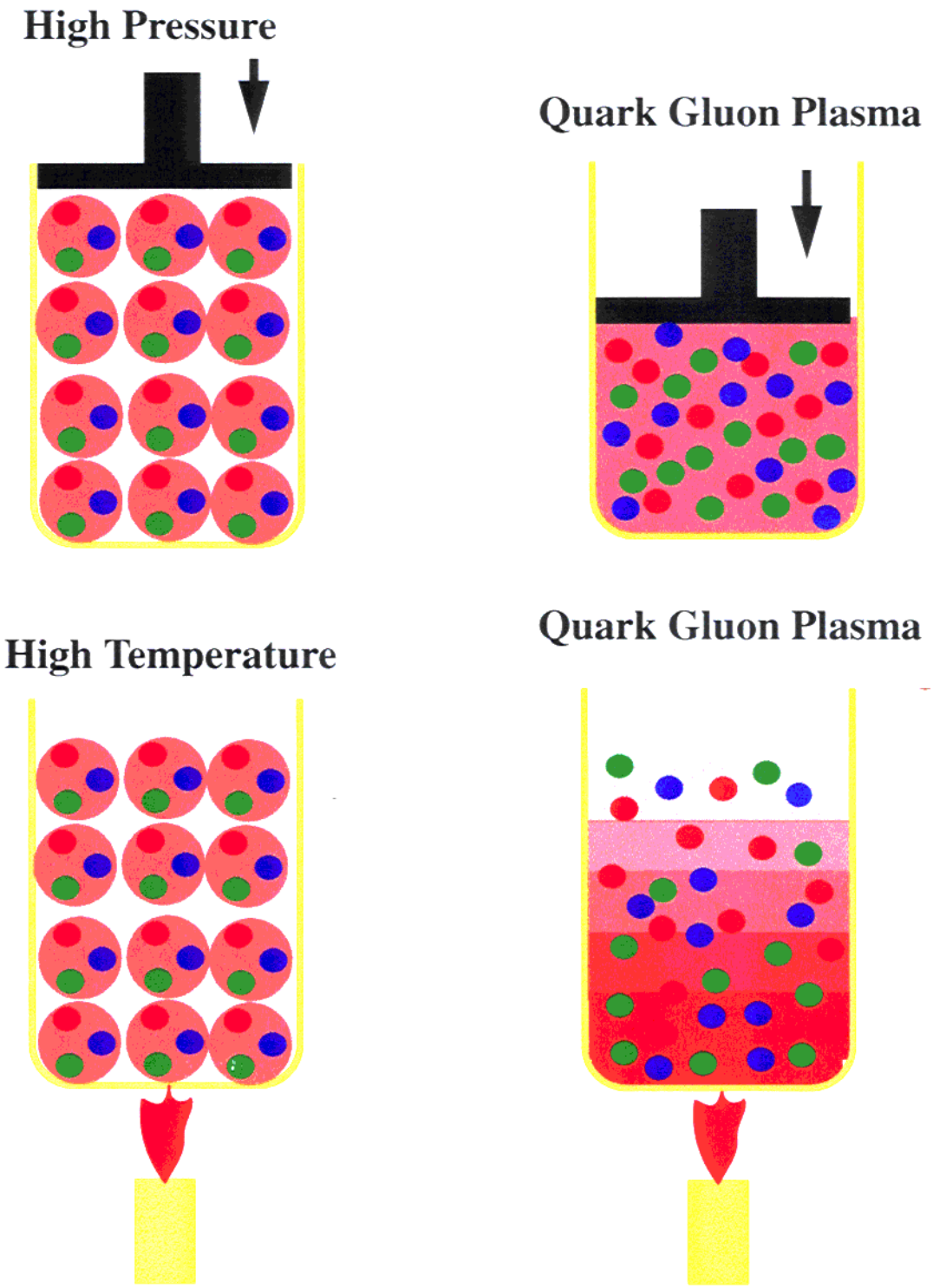
High Pressure
Quark Gluon Plasma
High Temperature
Quark Gluon Plasma

Figure 4

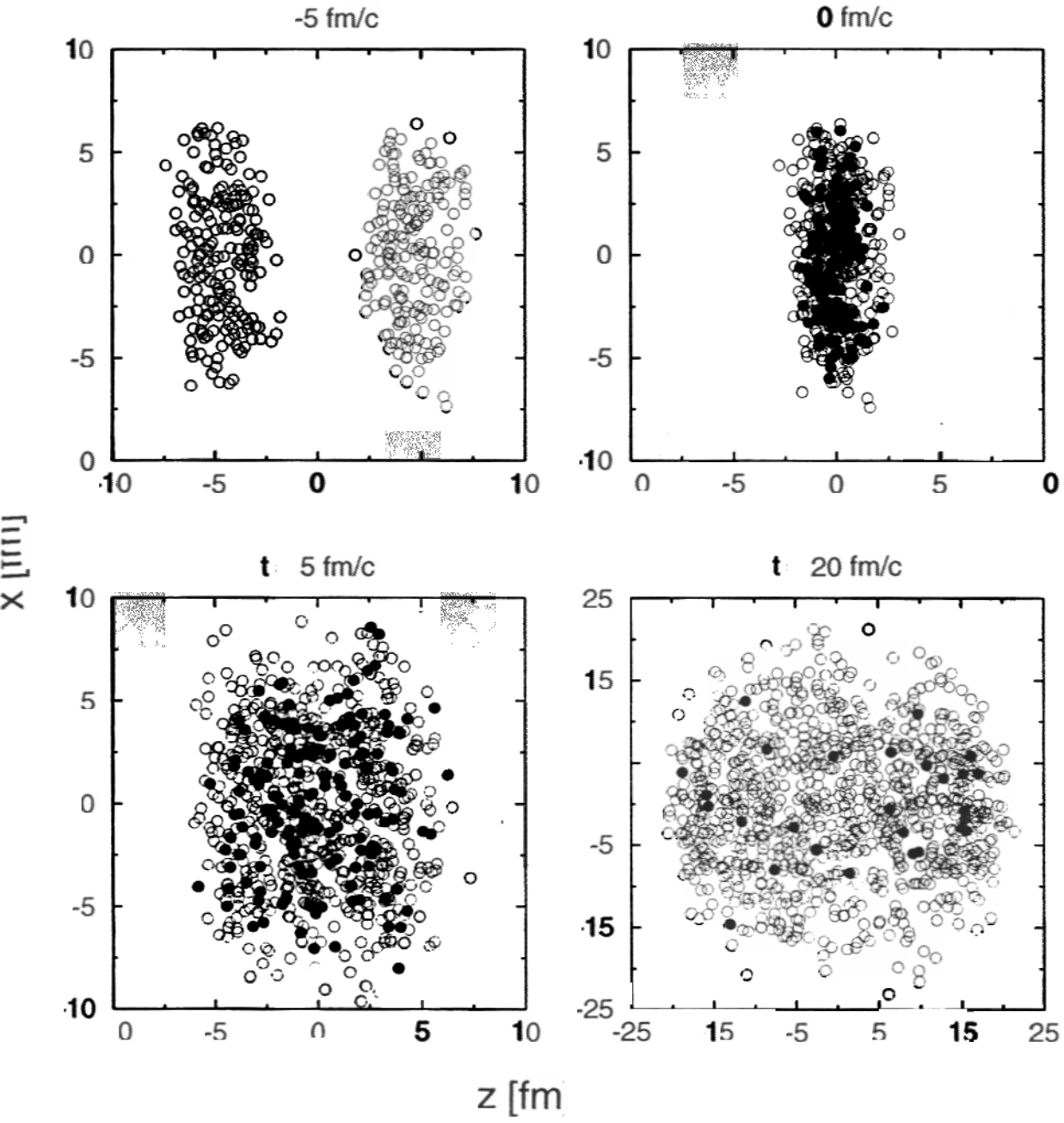

Figure 5

E866 Spectrometer

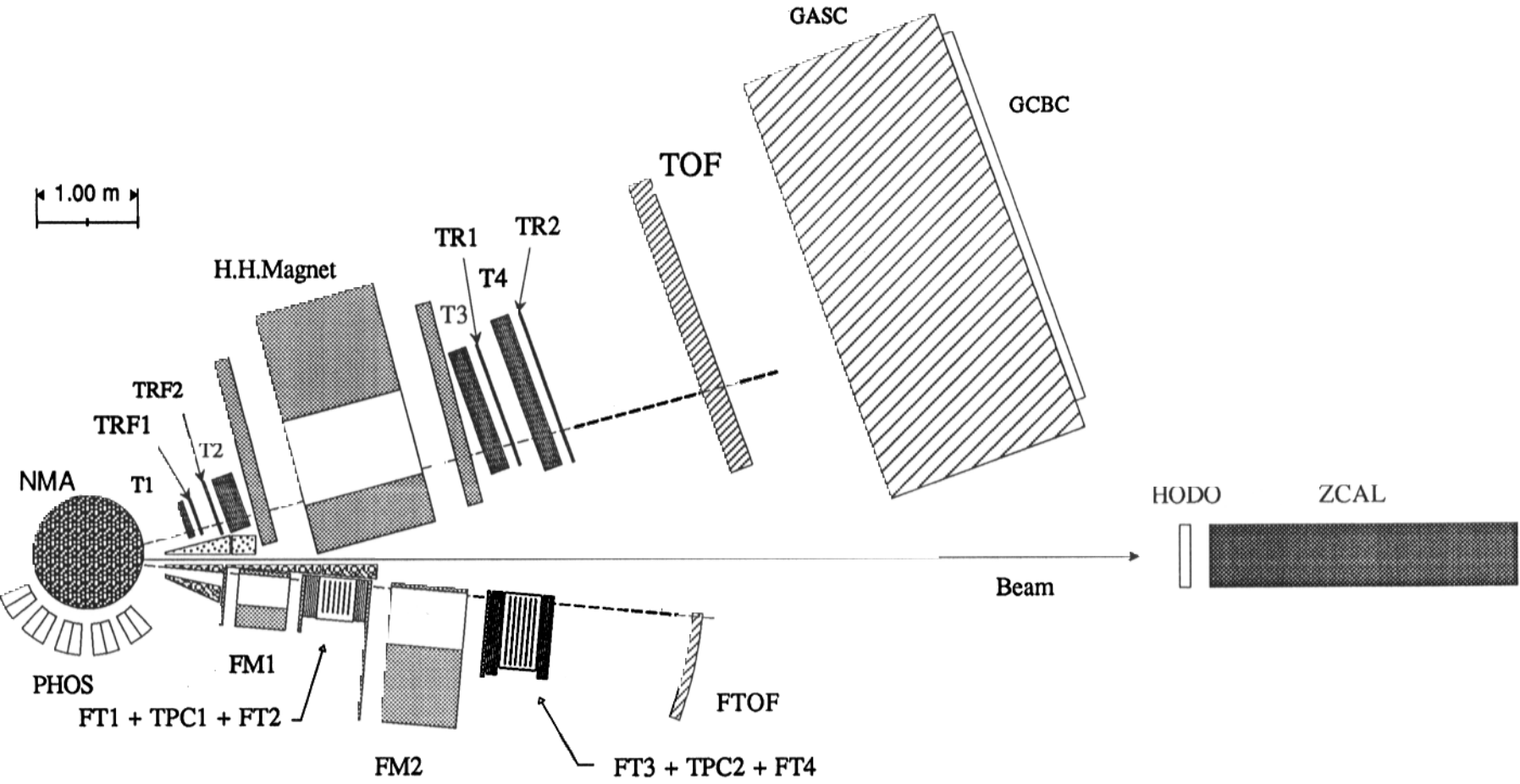

Figure 6

Correlation between ZCAL and NMA in E866 for Au+Au at 11.6 A GeV/c

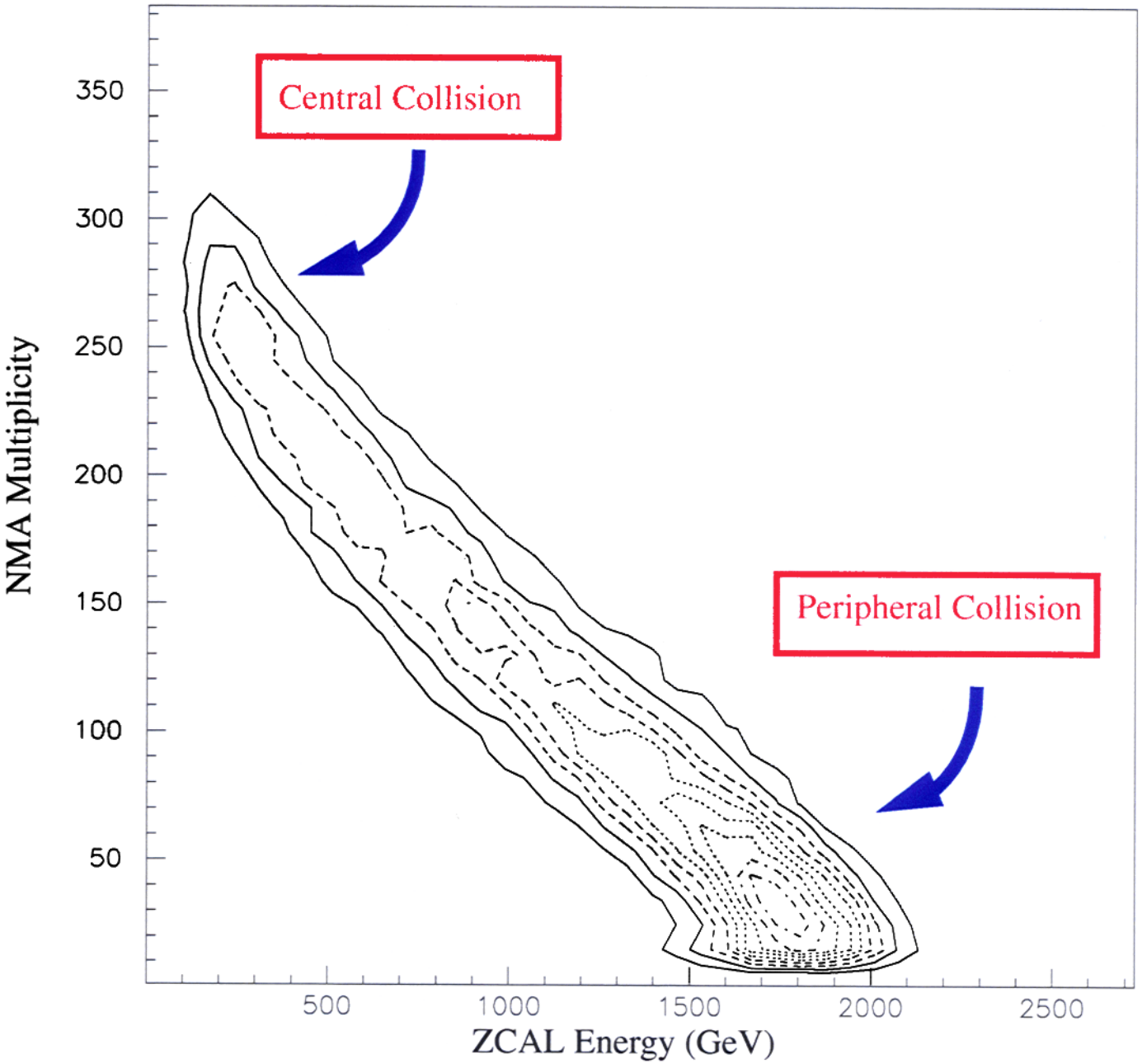

Figure 7

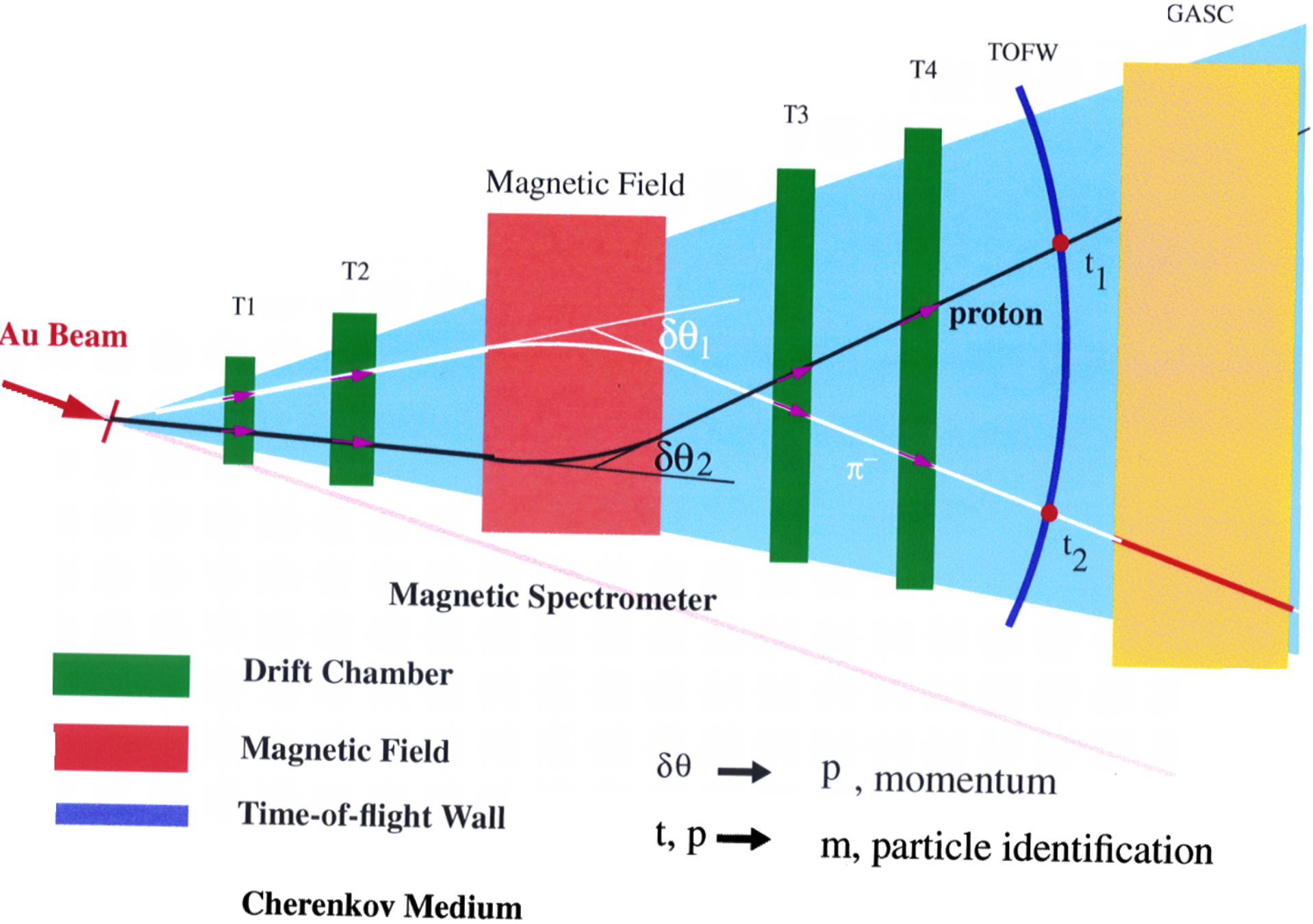
GASC
TOFW
T4
T3
Magnetic Field
T2
T1
Au Beam
$\delta\theta_1$
proton
t_1
$\delta\theta_2$
π^-
t_2
Magnetic Spectrometer
Drift Chamber
Magnetic Field
Time-of-flight Wall
Cherenkov Medium
$\delta\theta$ → p , momentum
t, p → m, particle identification

Measured variables for each particles:

p: momentum

m: mass

θ : emission angle

$y = y_{nn} + y'$

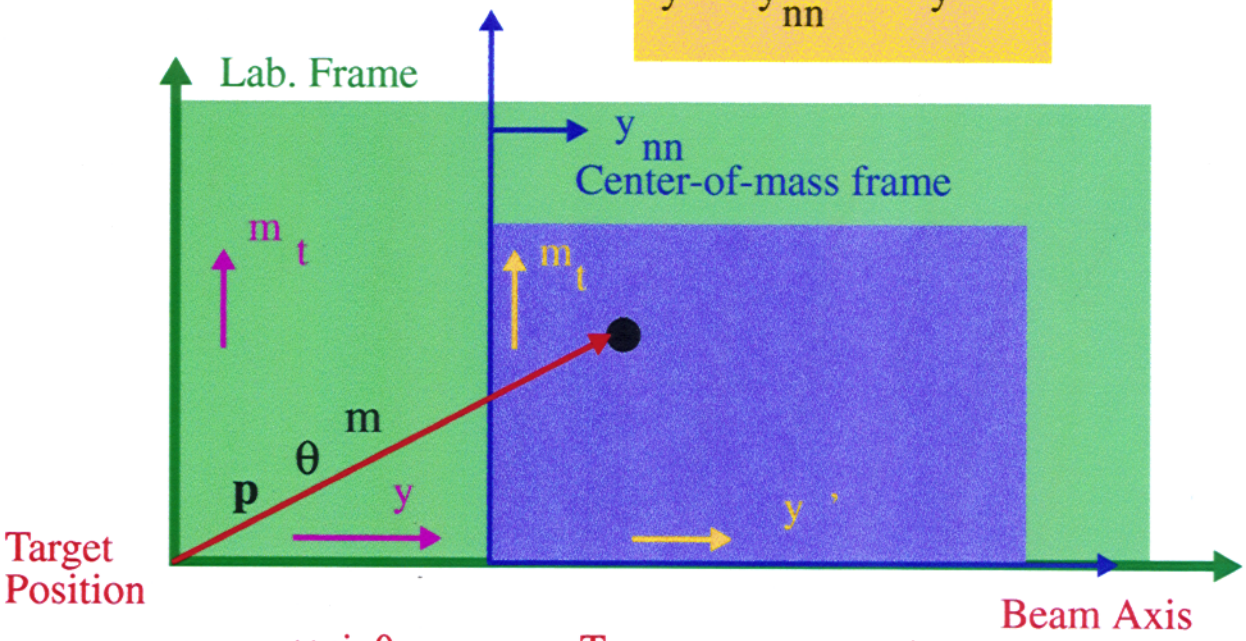

$p_t = p \times \sin\theta$ Transverse momentum

$p_p = p \times \cos\theta$ Parallel momentum

$e = \sqrt{p^2 + m^2}$ Energy

$m_t = \sqrt{p_t^2 + m^2}$ Transverse mass

$y = \frac{1}{2} \times \log\frac{e + p_p}{e - p_p}$ Rapidity

$e \times \frac{d\sigma}{dp^3}$ Invariant Cross-Section

Figure 9

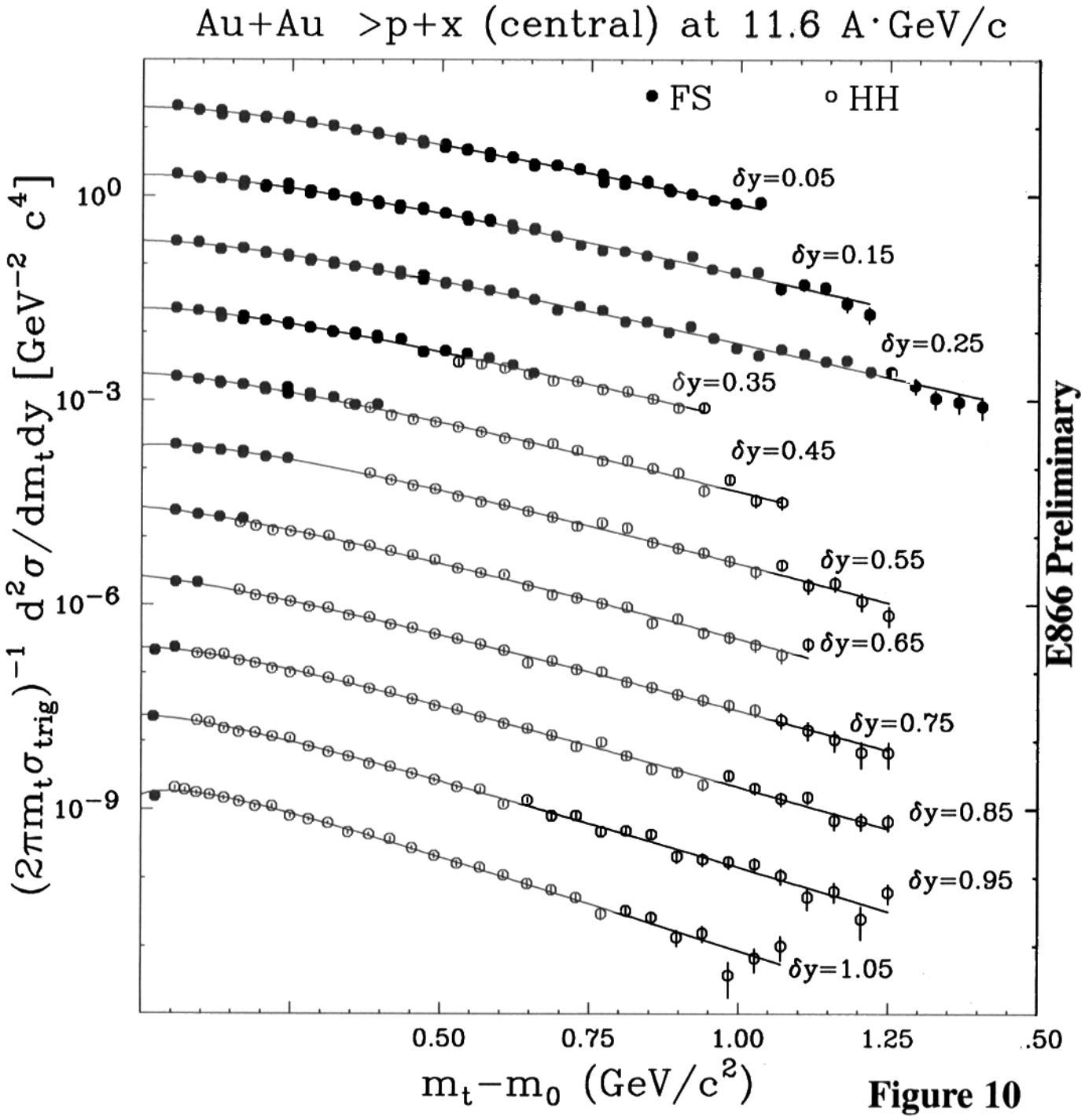
Au+Au >p+x (central) at 11.6 A·GeV/c
FS
HH
δy=0.05
δy=0.15
δy=0.25
δy=0.35
δy=0.45
δy=0.55
δy=0.65
δy=0.75
δy=0.85
δy=0.95
δy=1.05
10^0
10^{-3}
10^{-6}
10^{-9}
$(2\pi m_t \sigma_{trig})^{-1}\ d^2\sigma/dm_t dy\ [GeV^{-2}\ c^4]$
0.50
0.75
1.00
1.25
$m_t - m_0\ (GeV/c^2)$
E866 Preliminary

Figure 10

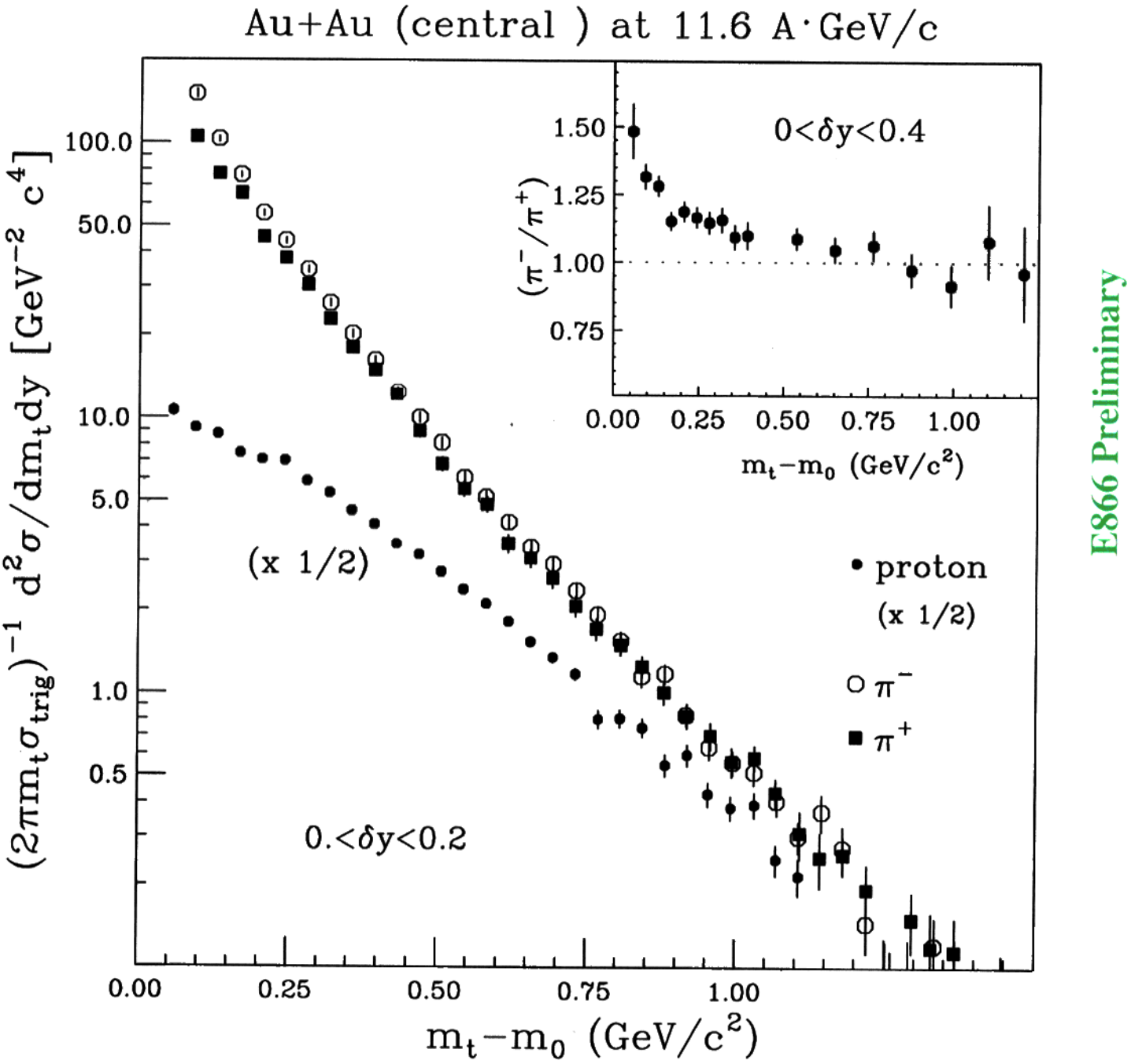
Au+Au (central) at 11.6 A·GeV/c
$(2\pi m_t \sigma_{trig})^{-1}\ d^2\sigma/dm_t dy\ [GeV^{-2}\ c^4]$
100.0
50.0
10.0
5.0
1.0
0.5
(x 1/2)
0.<δy<0.2
proton
(x 1/2)
π⁻
π⁺
0.00
0.25
0.50
0.75
1.00
$m_t - m_0$ (GeV/c^2)
0<δy<0.4
(π^-/π^+)
1.50
1.25
1.00
0.75
0.00
0.25
0.50
0.75
1.00
$m_t - m_0$ (GeV/c^2)
E866 Preliminary

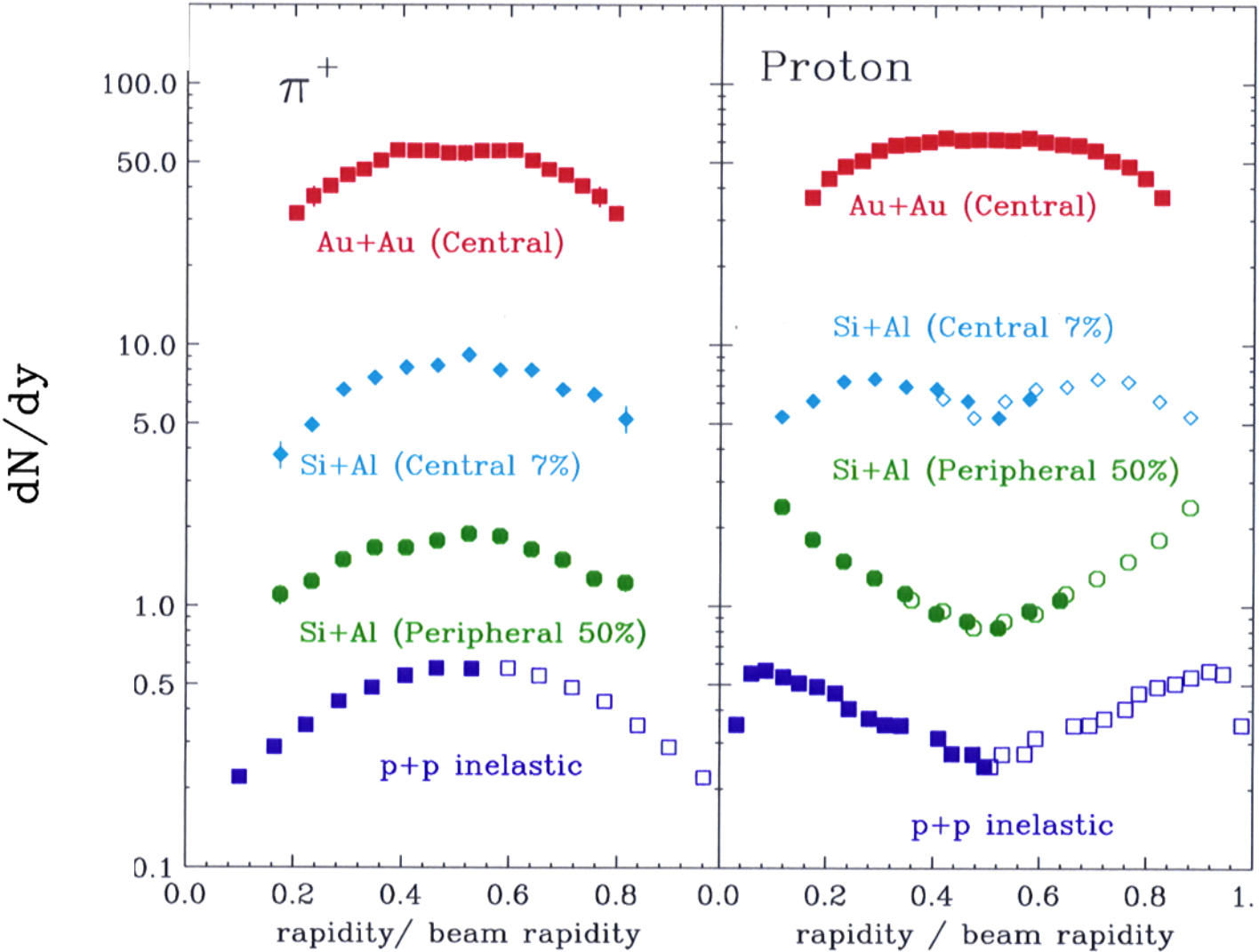
π+
Proton
Au+Au (Central)
Si+Al (Central 7%)
Si+Al (Peripheral 50%)
p+p inelastic
dN/dy
100.0
50.0
10.0
5.0
1.0
0.5
0.1
0.0
0.2
0.4
0.6
0.8
1.
rapidity/ beam rapidity
rapidity / beam rapidity

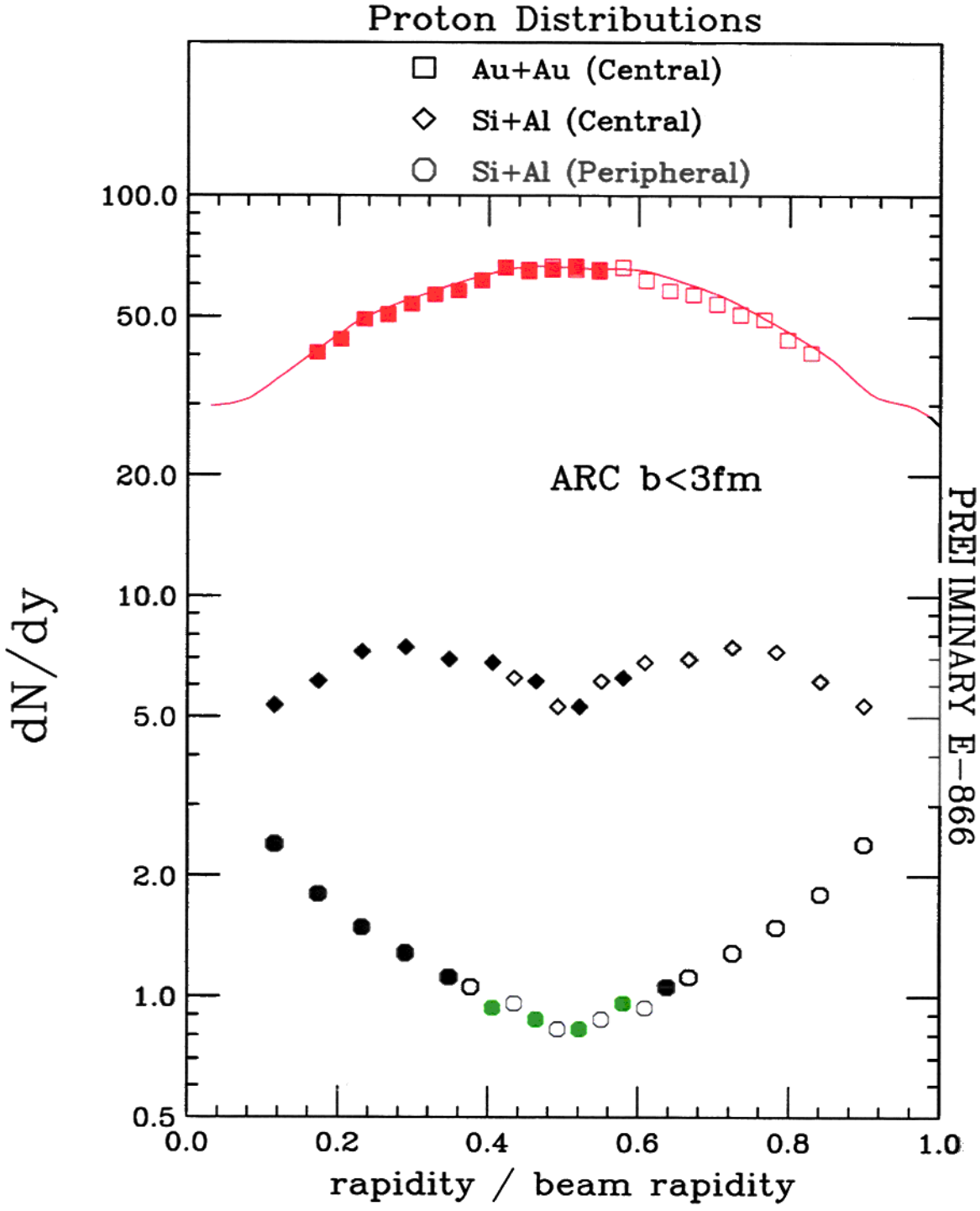
Proton Distributions
Au+Au (Central)
Si+Al (Central)
Si+Al (Peripheral)
ARC b<3fm
PRELIMINARY E-866
dN/dy
rapidity / beam rapidity
100.0
50.0
20.0
10.0
5.0
2.0
1.0
0.5
0.0
0.2
0.4
0.6
0.8
1.0

Figure 13

Central Au + Au at RHIC

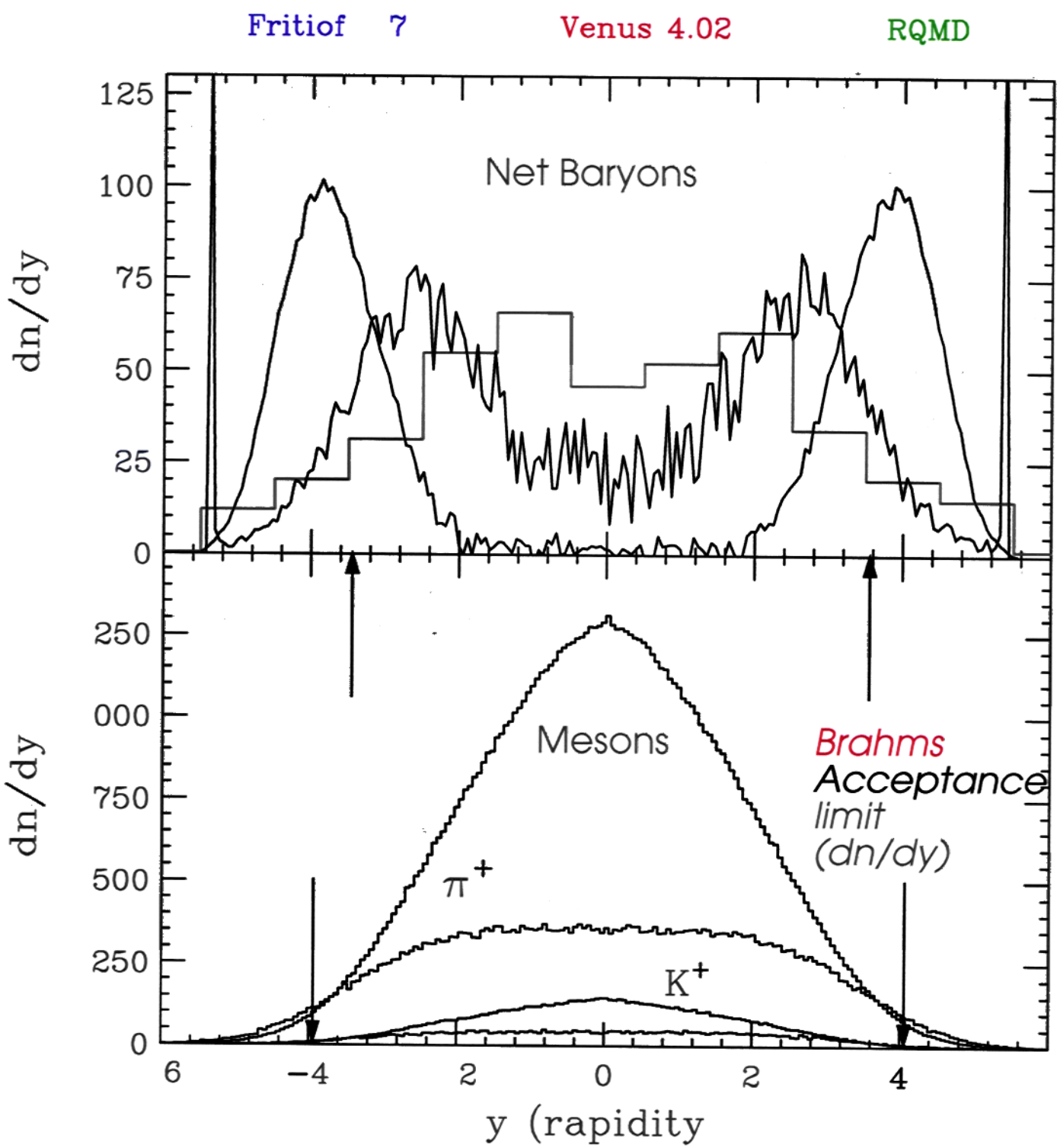

Figure 14

Acceptance of BRAHMS

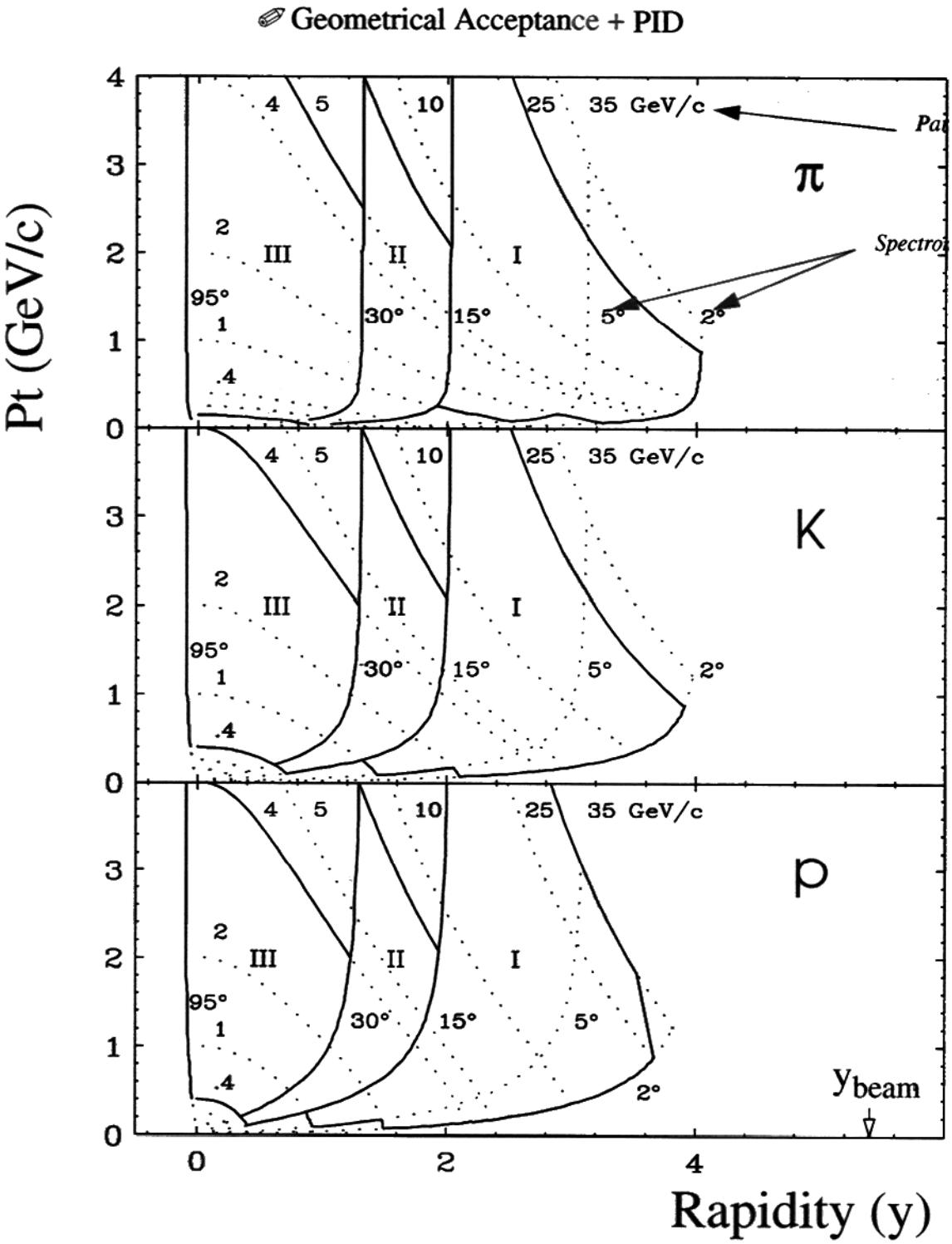

Region I : With the full Forward Arm
Region II : With the D1 - D2 (Forward Arm) Complex alone
Region III : With the Mid-Rapidity Arm

Figure 15

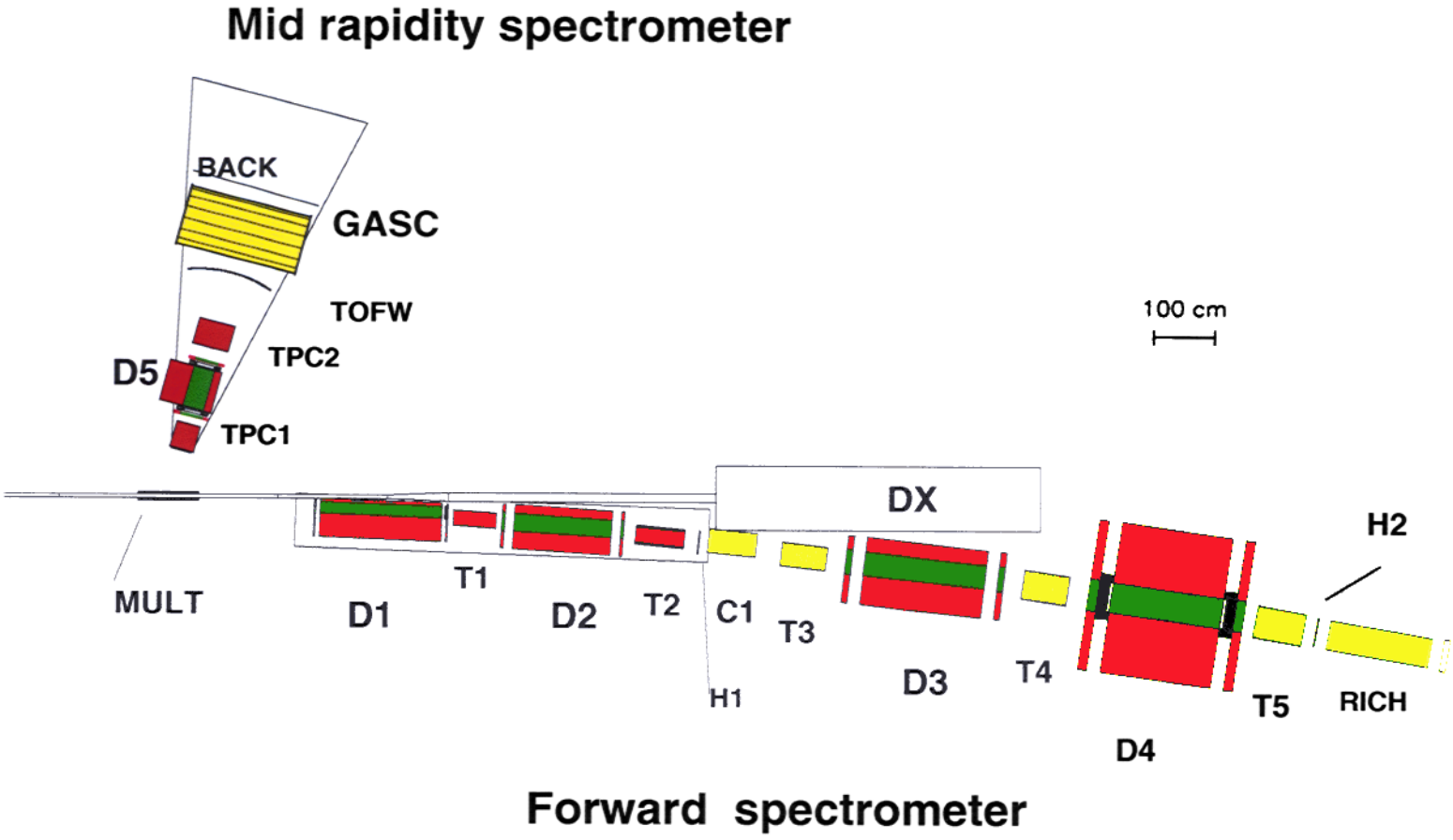
Mid rapidity spectrometer
BACK
GASC
TOFW
TPC2
D5
TPC1
100 cm
DX
H2
MULT
T1
D1
D2
T2
C1
T3
H1
D3
T4
T5
RICH
D4
Forward spectrometer

Figure 16